AIAA JOURNAL
Vol. 33, No. 6, June 1995

Flow Features of Shock-Induced Combustion Around Projectile Traveling at Hypervelocities

Akiko Matsuo* and Kozo Fujii†
Institute of Space and Astronautical Science, Sagamihara, Kanagawa 229, Japan
and
Toshi Fujiwara‡
Nagoya University, Nagoya, Aichi 464-01, Japan

The shock-induced combustion with periodic unsteadiness around a projectile fired into hypersonic flows is numerically studied. The mechanism of periodic unsteadiness is clarified using an x–t diagram of the flow variable on the stagnation streamline. The frequencies of the periodic unsteadiness obtained quantitatively agree with the experimental observations. The key parameters which are responsible in triggering the instability and in determining the frequency of the periodic unsteadiness are discussed by using the time integration of the species equations. The result indicates that the key parameters are induction time, heat release, and concentration of the heat release. The induction time is a key parameter for the frequency of the unsteadiness. The concentration of heat release is important for the unsteadiness itself. Total energy creating the compression waves depends on the amount of heat release itself. All of these features are recognized in a simple zero-dimensional analysis.

Introduction

THE computational approach is becoming widely used for many engineering problems. For the last few years, simulation[1–3] of hypersonic flows, including chemical reactions, has become one of the most advanced research topics in computational fluid dynamics (CFD) because such flows are difficult to physically realize in experimental apparatus such as wind tunnels. Many kinds of numerical techniques, which include the chemical reaction in high-temperature air, have been developed for the investigation of re-entry problems for space vehicles. Flows inside air-breathing engines have also been a target for study. For such internal flows, chemical reactions between fuel and oxygen occur and, generally, the stiffness of the reactions makes the simulation difficult. Some techniques were developed to avoid such difficulty in numerical simulations. Nowadays, the computational technique allows us to discuss the flow physics based on the simulation results, and we can find the detailed phenomena associated with the chemical reacting flow using CFD. In the present paper, one of the famous phenomena in shock-induced combustion is numerically investigated to clarify the underlying physics in detail.

Previous Work for Periodic Unsteadiness in Shock-Induced Combustion

Figures 1a and 1b are shadowgraph images of shock-induced combustion with the periodic unsteadiness around the hemispherical body taken by Lehr[4] in 1971. The projectile is flying at 1931 m/s in Fig. 1a and 1685 m/s in Fig. 1b in a hydrogen/air mixture of 293 K and 0.421 atm. The corrugated pattern on the reaction boundary is generated in front of the projectile body. The frequencies are 712 and 148 KHz, respectively. Similar periodic unsteadiness is observed in other experiments[5–8] where the projectiles are fired into premixed gas mixtures at Mach numbers around 4–6. A model of this periodic instability mechanism was proposed by McVey and Toong[5] using the x–t diagram between the bow shock and reaction front on the stagnation streamline on the basis of experimental observations and one-dimensional wave interaction theory. According to their work,[5] the generation mechanism is dominated by the wave interaction along the stagnation streamline in front of the projectile.

The generation mechanism of the periodic unsteadiness was numerically investigated by Matsuo and Fujiwara[9] in 1991. In the investigation, a simplified two-step model[10,11] is used to describe the chemical reaction instead of the realisitic elementary reactions. Based on the computed result, an improved model for the mechanism of the periodic unsteadiness was proposed. Figure 2 is the x–t diagram proposed by the authors.[9] This model includes the whole region between the stagnation point and the bow shock on the stagnation streamline. As in the proposed mechanism by McVey and Toong[5] based on the experimental observation, compression waves generated at a new reaction region have an important role for the periodic mechanism. It is verified by the investigation, on the other hand, that one of the generated compression waves propagates toward the stagnation point on the body surface, in addition to the compression waves toward the bow shock, which finally results in a contact discontinuity for the wave interaction with the bow shock wave. New reaction fronts are formed as a peninsula in the induction reaction region. Although this cyclic mechanism is generated by the compression waves created at the new reaction region, the compression waves are not always effective to produce the new reaction, depending on the strength of the compression wave. It should be noted that this improved model was proposed based on computed results using the simplified chemical reaction model, and the computed conditions are different from the experimental ones.

Dependency of frequency on the flying speed was also investigated by the present authors.[12] The cyclic mechanism depends on the relation between the shock stand-off distance and induction length, so that a periodic unsteadiness may be observed when certain conditions are satisfied. The computed result suggested that the relation between the chemical induction length (ignition delay time) and the shock stand-off distance was important in determining the frequency of the periodic unsteadiness. It was explained that the mechanism is basically dominated by the wave interaction and, thus, the same type of unsteady phenomenon occurred in the other combustible gas mixture.

Wilson and Sussman[13] have investigated shock-induced combustion with periodic unsteadiness by numerical simulation. They reproduced the flow pattern observed in Lehr's experiments using the same gas mixture under the same flow conditions as in his

Received Nov. 14, 1992; presented as Paper 93-0451 at the AIAA Aerospace Sciences Meeting, Reno, NV, Jan. 11–14, 1993; revision received Sept. 13, 1994; accepted for publication Nov. 28, 1994.

*Research Fellow of the Japan Society for the Promotion of Science; currently Research Associate, Department of Mechanical Engineering, Keio University. Member AIAA.
†Associate Professor, High-Speed Division. Member AIAA.
‡Professor, Department of Aeronautical Engineering. Member AIAA.

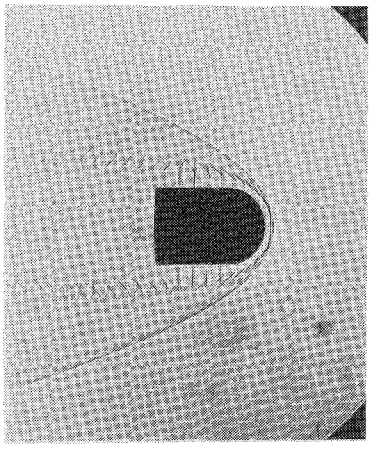

a)

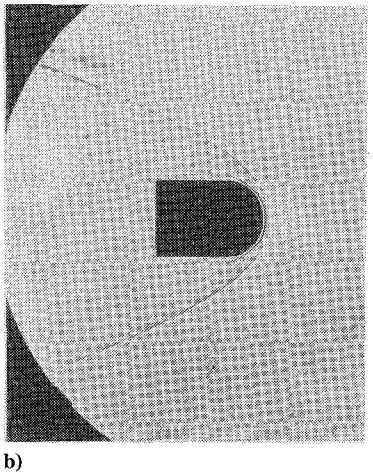

b)

Fig. 1 Shadowgraph of a spherical nose projectile moving into a premixed stoichiometric H_2/air mixture (courtesy of Lehr[4]): a) $v_{projectile}$ = 1931 m/s and b) $v_{projectile}$ = 1685 m/s.

experiment. They used the Euler equations with the logarithmic form of the species conservation equations as the governing equations. All of the terms (convective and chemical) are time integrated in a fully implicit manner. The mechanism of the unsteadiness on the stagnation streamline simulated by their work[13] shows a similar wave interaction to that in Fig. 2. However, the frequency of the periodic unsteadiness for the projectile speed of 1931 m/s was reported to vary from 530 to 820 KHz. They concluded that the uncertainties in the rate constants for the reaction mechanism could explain the differences of the frequency between the experiment and the computation because two kinds of the reaction rate constant were used for the simulation. Their work indicated that the effect of the characteristics of the selected rate constants is not negligible for the computation of such a supersonic combustion flowfield.

The mechanism of periodic unsteadiness in shock-induced combustion observed in the experiments is becoming clear by these recent works. However, the key parameters to trigger the instability and the frequency of the periodic unsteadiness have not been determined. To find the key parameters, Lehr's experiments are first simulated for the qualitative discussion of the mechanism in this paper. Then, the reaction profiles under Lehr's experimental condition are calculated by the zero-dimensional time integration of the species equations to clarify the characteristics. Finally, the effect of the ratio of the chemical scale with respect to the projectile body scale is examined by changing the projectile body size.

Mathematical Formulation

Simulations are conducted using the Euler equations with the species conservation equations under the axisymmetric assumption. The equations are integrated explicitly, and the chemical reaction source terms are treated in a linearly point-implicit manner. As a

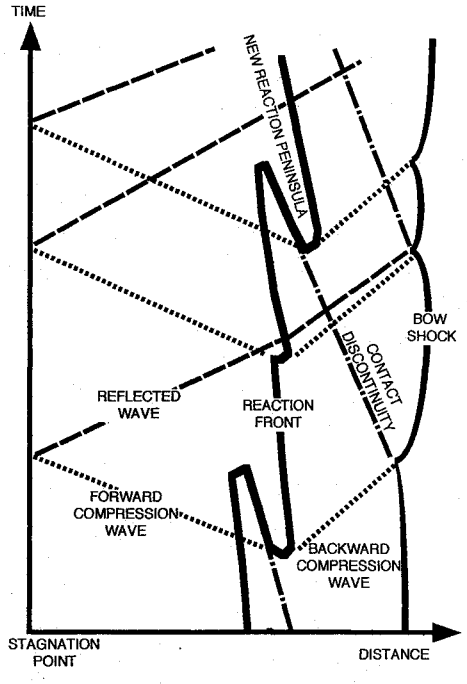

Fig. 2 Mechanism of the periodic unsteadiness by x–t diagram on the stagnation streamline.

numerical scheme, Yee's non-MUSCL type total variation diminishing (TVD) explicit scheme[14] is used. A fine grid distribution, such as 161 × 321 is used since the low amplitude and weak waves in front of the projectile are important. Since the phenomenon is unstable after the bow shock wave, an equally spaced grid is adopted along both directions.

The governing system of equations is written for inviscid flows and axisymmetric geometry

$$\frac{\partial \hat{Q}}{\partial \tau} + \frac{\partial \hat{E}}{\partial \xi} + \frac{\partial \hat{F}}{\partial \eta} = \hat{S} + \hat{H}$$

where $\hat{E}$ and $\hat{F}$ are the inviscid flux vectors in the ξ and η directions, respectively. $\hat{S}$ is the chemical reaction source vector, and $\hat{H}$ is the axisymmetric term. The inviscid flux vector and the chemical source vector are

$$\hat{Q} = J^{-1}\begin{pmatrix} \rho \\ \rho u \\ \rho v \\ e \\ \rho_i \end{pmatrix}, \qquad \hat{E} = J^{-1}\begin{pmatrix} \rho U \\ \rho u U + \xi_x p \\ \rho v U + \xi_y p \\ (e+p)U \\ \rho U_i \end{pmatrix}$$

$$\hat{F} = J^{-1}\begin{pmatrix} \rho V \\ \rho u V + \eta_x p \\ \rho v V + \eta_y p \\ (e+p)V \\ \rho V_i \end{pmatrix}, \qquad \hat{S} = J^{-1}\begin{pmatrix} 0 \\ 0 \\ 0 \\ 0 \\ \omega_i \end{pmatrix}$$

$$\hat{H} = J^{-1}\frac{\rho v}{y}\begin{pmatrix} 1 \\ u \\ v \\ (e+p)/\rho \\ 1 \end{pmatrix}$$

and

$$U = \xi_x u + \xi_y v, \qquad V = \eta_x u + \eta_y v$$

Reaction Mechanism

The oxyhydrogen combustion mechanism used in this study is taken from the work of Wilson and MacCormack[2] and Wilson and

Table 1 H_2/air combustion mechanism

i	Reaction	A	n	E
(1)	$H_2 + O_2 = HO_2 + H$	1.00×10^{14}	0	56,000
(2)	$H + O_2 = OH + O$	2.60×10^{14}	0	16,800
(3)	$O + H_2 = OH + H$	1.80×10^{10}	1	8,900
(4)	$OH + H_2 = H + H_2O$	2.20×10^{13}	0	5,150
(5)	$OH + OH = O + H_2O$	6.30×10^{12}	−2	1,090
(6)	$H + OH + M = H_2O + M$	2.20×10^{22}	−1	0
(7)	$H + H + M = H_2 + M$	6.40×10^{17}	−0.6	0
(8)	$H + O + M = OH + M$	6.00×10^{16}	0	0
(9)	$H + O_2 + M = HO_2 + M$	2.10×10^{15}	0	−1,000
(10)	$O + O + M = O_2 + M$	6.00×10^{13}	0	−1,800
(11)	$HO_2 + H = OH + OH$	1.40×10^{14}	0	1,080
(12)	$HO_2 + H = H_2O + O$	1.00×10^{13}	0	1,080
(13)	$HO_2 + O = O_2 + OH$	1.50×10^{13}	0	950
(14)	$HO_2 + OH = H_2O + O_2$	8.00×10^{12}	0	0
(15)	$HO_2 + HO_2 = H_2O_2 + O_2$	2.00×10^{12}	0	0
(16)	$H + H_2O_2 = H_2 + HO_2$	1.40×10^{12}	0	3,600
(17)	$O + H_2O_2 = OH + HO_2$	1.40×10^{13}	0	6,400
(18)	$OH + H_2O_2 = H_2O + HO_2$	6.10×10^{12}	0	1,430
(19)	$H_2O_2 + M = OH + OH + M$	1.20×10^{17}	0	45,500

$k_f = AT^n \exp(-E/RT)$; units are in seconds, moles, centimeters^3, calories, and kelvins.
Third body efficiencies relative to N_2: Reaction (6) $H_2O = 6.0$, Reaction (7) $H_2O = 6.0$; $H_2 = 2.0$, Reaction (8) $H_2O = 5.0$, Reaction (9) $H_2O = 16.0$; $H_2 = 2.0$, Reaction (19) $H_2O = 15.0$.

Sussman.[13] This reaction set was developed for supersonic combustion, and it basically consists of 13 reacting species (H_2, O_2, H, O, OH, H_2O, HO_2, H_2O_2, N, NO, NO_2, HNO, and N_2) and 33 reactions and is a modified Jachimowski's combustion mechanism.[15] However, this study uses only 8 species (H_2, O_2, H, O, OH, H_2O, HO_2, and H_2O_2) and 19 reactions, which are given in Table 1, to describe the combustion mechanism because the nitrogen reactions are not important around Mach 5. Therefore, all of the nitrogen reactions are omitted in this study, although the species N, NO, and HNO become important at higher Mach numbers.

For the calculation of species-specific heat, the thermodynamics data and their curve fit coefficients developed at the NASA Thermochemical Polynomials[16] are used.

Simulations of Lehr's Experiments

A flow condition for the first computation was selected to be the same as that of Fig. 1. The pressure and temperature in the gas mixture are set to be 0.421 atm and 293 K. Both 1931- and 1685-m/s projectile speeds are simulated using the Euler equations with the species conservation equations under the axisymmetric assumption.

Projectile Velocity 1931 M/S

Figure 3a shows the instantaneous density contour plots of the computed result under the same conditions as the experiment of Ref. 4 in Fig. 1a. Periodic unsteadiness along the reaction boundary is observed. The interaction of compression waves in front of the projectile body is clearly observed in the instantaneous pressure contour plots in Fig. 3b. At this instance, the compression waves, created by the new reaction which has just occurred around the stagnation streamline, move both toward the bow shock and the projectile body. Strong energy is released at the reaction boundary in front of the projectile body. However, no compression waves are observed in the downstream of the flowfield so that there should be no reaction progressing region. In order to confirm the reaction progressing region, the source term of water is plotted in Fig. 3c. Reaction mainly progresses along the reaction boundary and, especially, high reaction progress is observed in front of the projectile. The reaction progressing region is thought to create the compression waves and would be the trigger for the periodic unsteadiness.

To understand the mechanism of the periodic unsteadiness, it is useful to study the history of the variables on the stagnation streamline. Figure 4a is the history of the density distribution on the stagnation streamline. The wave interaction occurs not only between the bow shock and the reaction front but also between the reaction front and the projectile surface. The creation of the corrugated reaction peninsula is dominated by the wave interaction between the bow shock and the reaction front, although the compression wave reflected on the projectile surface also contributes in strengthening the compression wave released at the reaction front. Figure 4b is the history of the pressure distribution on the stagnation streamline. Only the compression waves are clearly observed. The new reaction zone in Fig. 4a obviously creates the compression waves both upstream and downstream, and the compression waves toward the projectile body is reflected at the body surface. The phenomena observed in Figs. 4 are exactly periodic. According to the experimental result of Lehr,[4] the period and the frequency of the oscillation are 1.405 μs and 712 KHz, respectively. In the present study, the period and the frequency are 1.38 μs and 725 KHz and the discrepancy of the period is less than 2%. Thus, the frequency of the periodic unsteadiness agrees well with the experimental observation. Although Wilson and Sussman[13] reported the frequency of the oscillation to be 820 KHz in their work, Wilson and Sussman[17] later obtained a frequency very close to the present result after continuing the computation for a longer time.

To compare it exactly with the experimental output of the shadowgraph image, the postprocessor[18] which simulates the three-dimensional shadowgraph system is used, and an output similar to the experiment is generated from the computational result. The result is shown in Fig. 5. Striations are observed in the reaction region, whereas no striations are observed in the density contour plots in Fig. 3a. This suggests that the striations in the reaction region in Fig. 1a are the three-dimensional images of the corrugated reaction boundary, and it is necessary to create the same output image as the experiment by integrating the light path. Because the striations in the reaction region was generated as observed in Fig. 1a by integrating the light path, it was confirmed that the axisymmetric assumption is acceptable.

Projectile Velocity 1685 M/S

As seen in Fig. 1b, the small amplitude oscillations with constant and low frequency along the reaction boundary are extremely weak. Figure 6a is the density contour plots of the simulated result under the experimental condition of Fig. 1b at the same speed. The calculated result in Fig. 6a also shows the weak wave interaction in front of the projectile body, and the extremely small corrugated pattern is observed on the reaction boundary. To clarify the phenomenon, the density gradient is plotted in Fig. 6b. The weak wave interaction, which is generated by the contact discontinuity, and the compression waves between the bow shock and reaction boundary and the corrugated pattern on the reaction boundary are clearly observed.

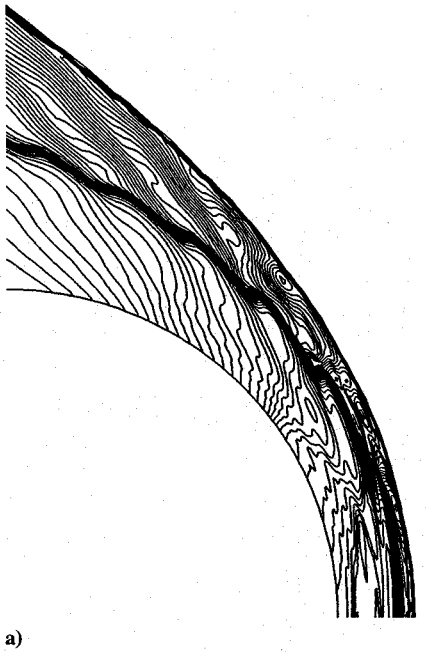

a)

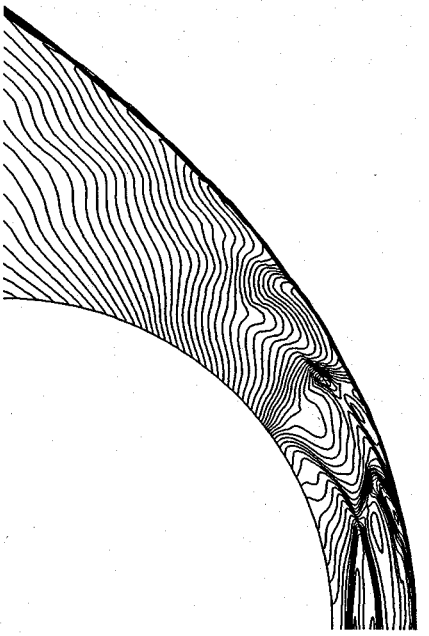

b)

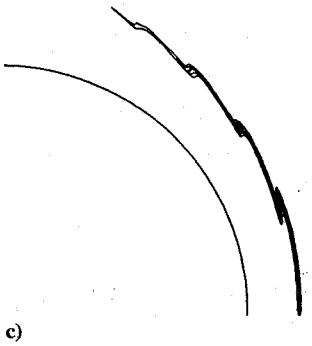

c)

Fig. 3 Contour plots for the projectile speed 1931 m/s: a) density, contour range min = 0.2, max = 2.2, inc = 0.03 kg/m^3; b) pressure, 0.01, 1.31, and 0.02 MPa; and c) ω_{water}.

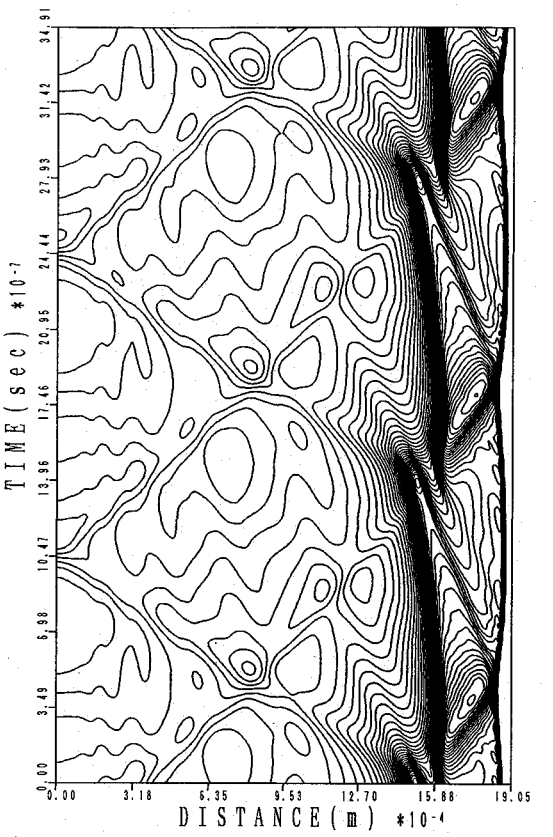

a)

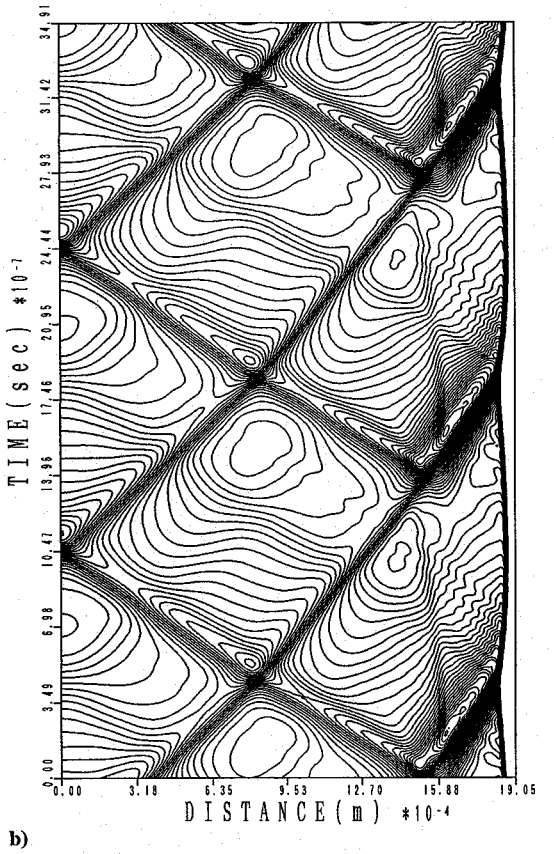

b)

Fig. 4 Histories of the density and pressure distributions on the stagnation streamline for the projectile speed 1931 m/s: a) density and b) pressure.

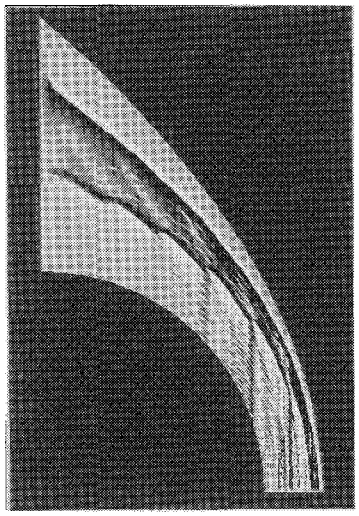

Fig. 5 Three-dimensional shadowgraph image[18] created from the computed result.

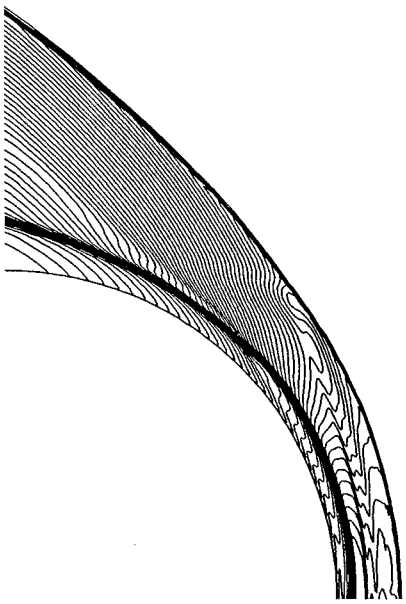

a)

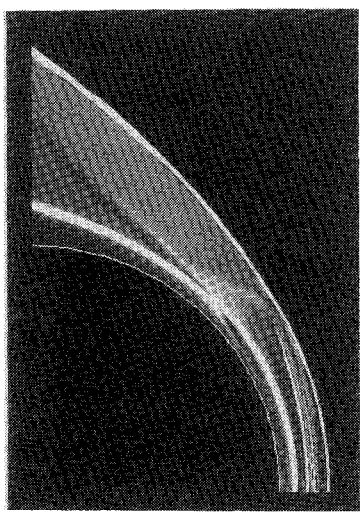

b)

Fig. 6 Plots for the projectile speed 1685 m/s: a) density, contour range min = 0.15, max = 0.9, inc = 0.025 kg/m^3; and b) density gradient.

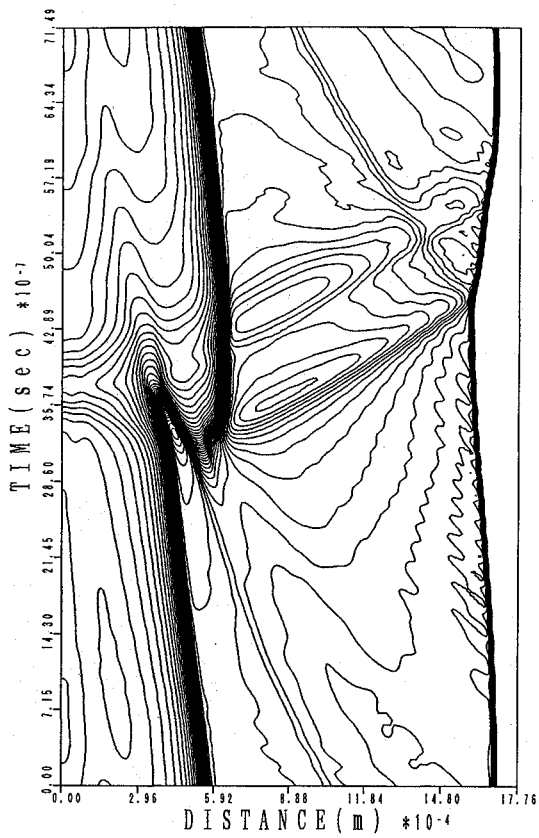

a)

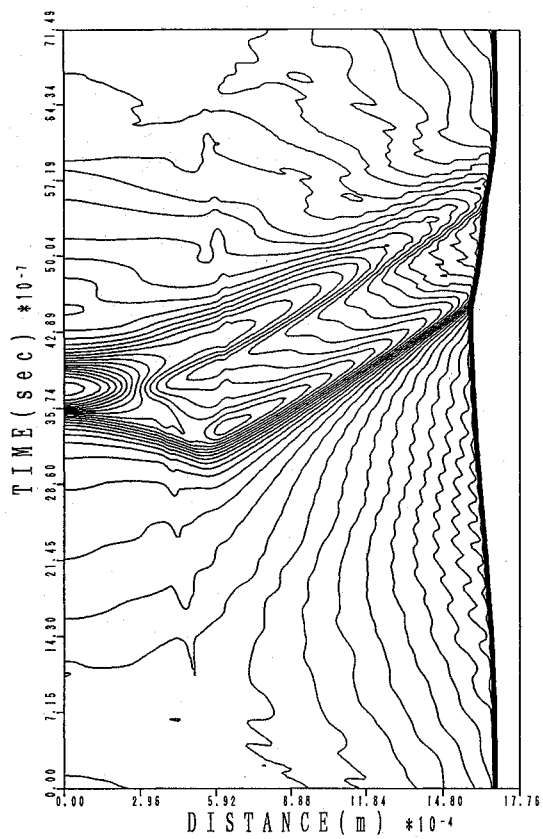

b)

Fig. 7 Histories of the density and pressure distributions on the stagnation streamline for the projectile speed 1685 m/s: a) density and b) pressure.

Figures 7a and 7b show the history of the density and the pressure distribution on the stagnation streamline. The density distribution shows the bow shock, the reaction front, the compression wave, and the contact discontinuity as are shown in Fig. 4a. The wave interaction in Fig. 7a can also be explained by the mechanism in Fig. 2 although reaction occurs much closer to the body in this case. The compression waves released at the new reaction region propagate to the upstream and downstream, and both compression waves interact with the bow shock and make the contact discontinuity. Basically two contact discontinuities are generated after the interaction. However, these contact discontinuities are closely and parallelly located and make one new reaction peninsula. One cycle of the periodic unsteadiness corresponds to 6.256 μs in this calculation, and the frequency is 159.8 KHz. Since the experimental result indicates that the frequency is 148 KHz, the agreement is also quite good in this case.

Discussion

From the plots of the numerical results in the preceding section, the mechanism of periodic unsteadiness in the shock-induced combustion of Lehr's experiments is now better understood. In addition, it suggested that such periodic unsteadiness is a universal phenomenon in shock-induced combustions and could occur in any gas mixture under appropriate conditions because the fluid dynamic wave interaction on the stagnation streamline is the cause for the unsteadiness. The periodic unsteadiness observed for the different gas mixtures in the authors' previous work is now considered to be of the same type of phenomenon as Lehr's experiment.[4]

Thus far, the key parameters for the periodic unsteadiness are as follows:

1) induction time (ignition delay time) on the stagnation streamline and the corresponding induction length, which determines frequency;

2) the compression wave reflected on the projectile surface, which may smear periodicity; and

3) the relative scale of the induction length and the shock stand-off distance, which determines the wave interaction pattern.

However, the effect of the characteristics of the chemical kinetics of gas-phase hydrogen-air combustion has not been discussed. The reaction profiles will be discussed in the next section.

Characteristics of Chemical Kinetics

The time integration of species equations in zero dimension in space under a constant volume mode is carried out in order to clarify the characteristics of the reaction profile in Table 1. We assume that all of the flow variables are given for the conditions after the bow shock on the stagnation streamline and that the flow speed corresponds to the projectile speed. The integration procedure is as follows.

1) Flow variables downstream of the normal shock wave are given as an initial condition by the Rankin–Hugoniot relation of the real gas.

2) All of the species equations are time integrated. During the reaction progress, total density change is not allowed under the constant volume mode.

For the calculation of the species-specific heat, the thermodynamics data and their curve fit coefficients developed at the NASA Thermochemical Polynomials[16] are used. This procedure provides accurate data for the characteristics of a nonequilibrium reaction under the constant volume mode. If the fluid velocity after the bow shock wave on the stagnation streamline is constant (without isentropic compressions), the induction reaction length is given. Consequently, the relation between the shock stand-off distance and the induction length is roughly estimated.

Two projectile speeds of 1685 and 1931 m/s, which were used in the present simulations, are tested. The conditions of the gas mixture are selected to fit Lehr's experiments.[4] As the exothermic reaction occurs after the ignition delay and causes a sudden temperature increase, the time-evolving temperature profiles are plotted in Fig. 8. The time period required for the temperature increase due to the exothermic reaction, called the reaction time, is almost the same for both cases. However, the induction times are 1.0 μs for

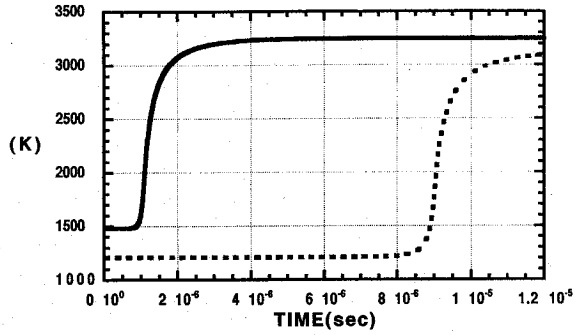

Fig. 8 Time-evolving temperature profiles: ——, 1931 m/s; - - -, 1685 m/s.

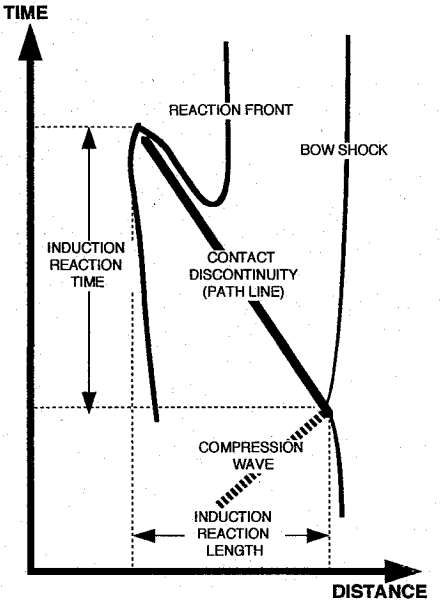

Fig. 9 Schematic picture showing the induction time and length in the history of the density distribution.

1931 m/s and 8.8 μs for 1685 m/s and a significant difference exists. The flow velocities after the bow shock computed by the Rankin–Hugoniot relation are 361.26 m/s for the 1931 m/s projectile speed and 340.35 m/s for the 1685-m/s projectile speed. The induction length is roughly calculated by multiplying the flow velocity $\times$ the induction time, if the isentropic compression is negligible. They are 0.36126 mm and 2.995 mm, respectively. The induction times and lengths in the actual simulations can be measured in the manner shown in Fig. 9. Comparing Figs. 4a and 7a, the induction time and length in the real simulations are 1.0 ms and 0.36 mm for 1931 m/s, and 5.7 ms and 1.2 mm for 1685 m/s. The induction time and length of the projectile speed 1931 m/s in Fig. 4a exactly agree with those in the reaction profile in Fig. 8. As the induction length in Fig. 4a is only $\frac{1}{6}$ of the shock stand-off distance and contact discontinuities are straight, the effect of the isentropic compression can be neglected. However, the induction time and length of the projectile speed 1685 m/s in Fig. 7a do not agree with the reaction profile in Fig. 8.

As seen in Fig. 7a, the contact discontinuities, which indicate the particle path line, are not straight but curved due to the deceleration, isentropic compressions after the bow shock wave has to be considered in this case. Thus, the discrepancy may come from the effect of isentropic compression during the induction length that occupies $\frac{2}{3}$ of the shock stand-off distance.

This observation suggests that the induction time is one of the important key parameters that determines the frequency of the periodic unsteadiness. In addition, it was shown that frequency may be predicted from analysis of the zero-dimensional time integration of species equations without simulating the flowfield.

Projectile Diameter 2.5 mm

The mechanism of the periodic unsteadiness in the shock-induced combustion is much better understood through systematic simulation. In previous work[9] with the simplified two-step reaction model, the periodic unsteadiness was reported when the projectile radius is $10L^*$ (where L^* is the induction length of the plane C–J detonation). However, when a smaller projectile radius ($5L^*$) was used in the simulations, the unsteadiness disappeared from the flowfield. The absence of the unsteadiness has not been clarified so far. Therefore, the case for the smaller projectile body is simulated using a hydrogen/air gas mixture under the same condition of the projectile speed 1931 m/s for the quantitative discussion. The projectile diameter is selected to be 2.5 mm.

Figure 10a is the density contour plots of the aforementioned case of projectile diameter 2.5 mm and projectile speed 1931 m/s. The ratio of the shock stand-off distance with respect to the region of the burned gas on the stagnation streamline is almost the same as that in the case of the projectile speed 1685 m/s in Fig. 6a. However, no wave interaction on the stagnation streamline is observed in this case. Figure 10b is the pressure contour plot which only shows the smooth contour lines in the entire flowfield, even in front of the projectile. The steady solution is obtained in this simulation.

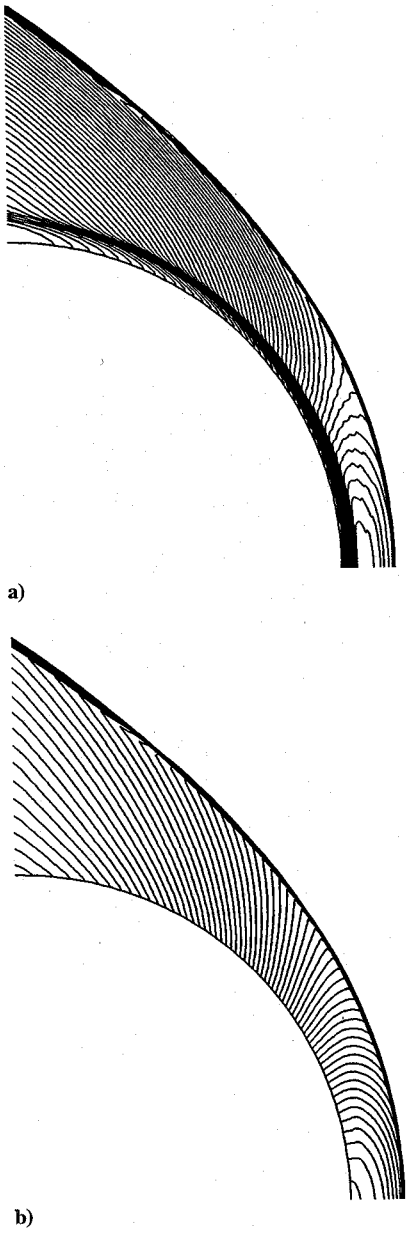

Fig. 10 Contour plots for the projectile diameter 2.5 mm and the speed 1931 m/s: a) density, contour range min = 0.2, max = 2.1, inc = 0.03 kg/m^3; and b) pressure 0.01, 1.3, and 0.02 MPa.

The relative location of the reaction boundary in Fig. 10a is almost the same as that in Fig. 6a. But one shows the periodic unsteadiness, and the other does not show it. This indicates that induction time is not solely the key parameter for the periodic unsteadiness. What is an important key parameter for the unsteadiness?

Profiles of the Stagnation Line

Case A

Case a with speed of 1931 m/s and diameter of 15.0 mm shows the periodic unsteadiness around the projectile body in the experimental (Fig. 1a) and computational results (Figs. 3–5). Figure 11a shows the temperature profile and the local temperature increase (dT/dx), which is the ratio of the local temperature increase with respect to the projectile scale, on the stagnation streamline. According to the

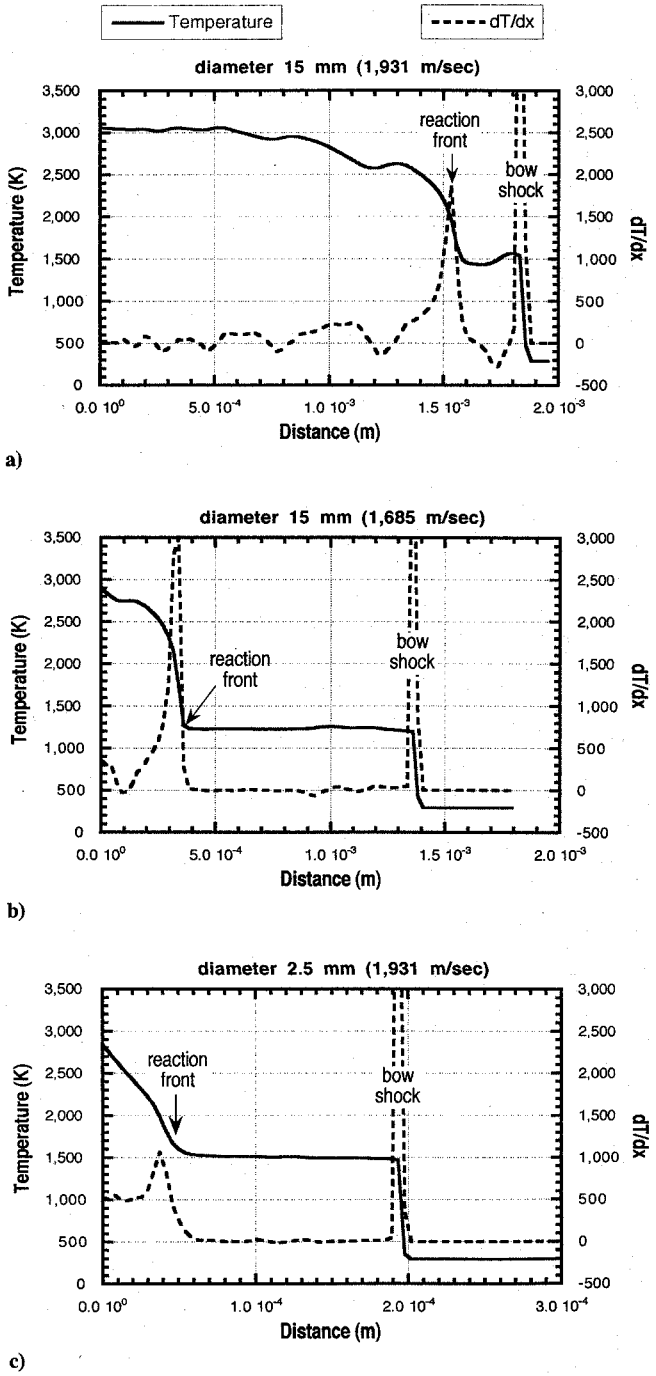

Fig. 11 Temperature profile and local temperature increase (dT/dx) on the stagnation streamline.

preceding section, the induction length is estimated by multiplying the flow velocity × the induction time. The induction length in Fig. 11a agrees with the estimation of the preceding section. In the local temperature increase, the peaks appear at the bow shock and the reaction front.

Case B

Case b with speed of 1685 m/s and diameter of 15.0 mm also shows the periodic unsteadiness in Figs. 1b, 6, and 7. As discussed in the preceding section, the induction length in this case can not be estimated by the characteristics of the chemical kinetics because of the isentropic compression. In Fig. 11b, the peaks of the local temperature increase (dT/dx) appear at the bow shock and the reaction front as well as in case a.

Case C

In case c, with speed of 1931 m/s and diameter of 2.5 mm, the simulated results are shown in Fig. 10 and unsteadiness is not observed. The flow features in Fig. 10a is similar to those in Fig. 6a. Figures 11b and 11c indicate the same ratio of the shock stand-off distance to the burned gas region. However, the profiles of the temperature increase (dT/dx) at the reaction front show different behavior. The local temperature increase corresponds to the nondimensionalized energy release by the fluid scale, then the value indicates the strength of the created wave. The profiles indicate that the energy release at the reaction front in case b is much stronger than that in case c. Therefore, the compression waves are created at the reaction front. These results suggest that the strength of the energy release changes the unsteadiness of the flowfield.

Key Parameters for Unsteadiness

We now examine the ratio of the reaction period, which is the length for the temperature increase, to the shock stand-off distance. It corresponds to the intensity of the concentration of the energy release by the exothermic reaction. Here, the term concentration of heat release indicates the ratio of the reaction period, which is the length or time for the temperature increase, to the shock stand-off distance. It does not mean heat release rate. The ratio of the reaction period to the shock stand-off distance in case c is much larger than that of cases a and b. Therefore, compression waves are created at the reaction front gradually rather than abruptly.

The key parameters are summarized in the following.

1) The first parameter is induction time (ignition delay time), which determines the frequency of the periodic unsteadiness.

2) Next is heat release, which is the temperature increase in the reaction period. In the simulation of the flowfield, the location of the bow shock is changed due to the heat release so that the path of the reflected compression waves is changed.

3) Concentration of heat release, which is given by the ratio of the reaction period to the shock stand-off distance, is an important parameter for unsteadiness.

Conclusion

A series of simulations clarified the key parameters of the periodic unsteadiness around the projectile traveling at hypervelocity. They are considered to be the induction time, the heat release, and the concentration of the heat release. The induction time is a key parameter for the frequency of unsteadiness. The concentration of the heat release is important for the unsteadiness itself. The amount of the heat release is important because the total energy creating the compression waves depends on it. Simple zero-dimensional analysis is useful because all these features can be recognized in such an analysis.

Acknowledgment

This research was supported in part by the Scientific Research Fund from the Ministry of Education awarded to the first author.

References

[1]Lee, S. H., and Deiwert, G. S., "Flux-Vector Splitting Calculation of Nonequilibrium Hydrogen-Air Reactions," *Journal of Spacecraft and Rockets*, Vol. 27, No. 2, 1990, pp. 167–174.

[2]Wilson, G. J., and MacCormack, R. W., "Modeling Supersonic Combustion Using a Fully Implicit Numerical Method," *AIAA Journal*, Vol. 30, No. 4, 1992, pp. 1008–1015.

[3]Yungster, S., Eberhardt, S., and Bruckner, A. P., "Numerical Simulation of Hypervelocity Projectiles in Detonable Gases," *AIAA Journal*, Vol. 29, No. 2, 1991, pp. 187–199.

[4]Lehr, H. F., "Experiments on Shock-Induced Combustion," *Astronautica Acta*, Vol. 17, 1972, pp. 589–597.

[5]McVey, J. B., and Toong, T. Y., "Mechanism of Instabilities of Exothermic Hypersonic Blunt-Body Flow," *Combustion Science and Technology*, Vol. 3, 1971, pp. 63–76.

[6]Alpert, R. L., and Toong, T. Y., "Periodicity in Exothermic Hypersonic Flow about Blunt Projectiles," *Astronautica Acta*, Vol. 17, 1972, pp. 539–560.

[7]Behrens, H., Struth, W., and Wecken, F., "Studies of Hypervelocity Firings into Mixtures of Hydrogen with Air or with Oxygen," *Tenth Symposium (International) on Combustion*, Combustion Inst., Pittsburgh, PA, 1965, pp. 245–252.

[8]Ruegg, F. W., and Dorsey, W., "A Missile Technique for the Study of Detonation Wave," *Journal of Research of the National Bureau of Standards*, Vol. 66C, No. 1, 1962, pp. 51–58.

[9]Matsuo, A., and Fujiwara, T., "Numerical Investigation of Oscillatory Instability Mechanism in Shock-Induced Combustion around an Axisymmetric Blunt Body," *AIAA Journal*, Vol. 31, No. 10, 1993, pp. 1835–1841.

[10]Korobeinikov, V. P., Levin, V. A., Markov, V. V. , and Chernyi, G. G., "Propagation of Blast Waves in a Combustible Gas," *Astronautica Acta*, Vol. 17, 1972, pp. 529–537.

[11]Taki, S., and Fujiwara, T., "Numerical Analysis of Two-Dimensional Nonsteady Detonation," *AIAA Journal*, Vol. 16, No. 1, 1978, pp. 73–77.

[12]Matsuo, A., Fujiwara, T., and Fujii, K., "On The Mechanism of Shock-Induced Combustion around an Axisymmetric Blunt Body," *Proceedings of the 18th International Symposium on Space Technology and Science* (Kagoshima, Japan), 1992, pp. 691–696.

[13]Wilson, G. J., and Sussman, M. A., "Computation of Unsteady Shock-Induced Combustion Using Logarithmic Species Conservation Equations," *AIAA Journal*, Vol. 31, No. 2, 1993, pp. 294–301.

[14]Yee, H. C., "Upwind and Symmetric Shock Capturing Schemes," NASA TM 89464, 1987.

[15]Jachimowski, C. J., "An Analytical Study of the Hydrogen-Air Reaction Mechanism With Application of Scramjet Combustion," NASA TP-2791, Feb. 1988.

[16]Wilson, G. J., "Computation of Steady and Unsteady Shock-Induced Combustion Over Hypervelocity Blunt Bodies," Ph.D. Thesis, Dept. of Aeronautics and Astronautics, Stanford Univ., Stanford, CA, Dec. 1991.

[17]Wilson, G. J., and Sussman, M. A., private communication, Eloret Institute, Palo Alto, CA, Oct. 1994.

[18]Tamura, Y., and Fujii, K., "Simulation of Experimental Visualization Methods for Computational Fluid Dynamics Research," *International Journal of Computational Fluid Dynamics*, Vol. 2, pp. 309–333.